ARQII Publication
http://arqiipubl.com/ams

APPLICATIONS OF
MODELLING AND SIMULATION

eISSN 2600-8084 VOL 4, 2020, 258-271

Numerical Design of a Guide Vane for an Axial Fan

Ali Saeidi[1] and Pooya Taheri[2*]

[1]Department of Mechanical and Manufacturing Engineering, Universiti Putra Malaysia, Serdang, Selangor, Malaysia
[2]Mechatronic Systems Engineering Department, Simon Fraser University, Surrey, BC, Canada

[*]Corresponding author: ptaherig@sfu.ca

Submitted 20 May 2020, Revised 27 June 2020, Accepted 01 July 2020.

Abstract: This study presents a custom guide vane design to substantially reduce the waste energy in axial fans. Ideally, there is no velocity component in the radial direction in axial fans, but in practice, the air leaving the axial fan has a large tangential component of velocity which produces a large amount of swirl kinetic energy. In order to solve this problem, a guide vane is designed to remove the rotational component of the air. The methodology described in this project is based on the fundamental governing continuity, momentum, and energy equations using the Finite Volume Method (FVM). In this project, the standard k-ω model is used for turbulent modeling. Two dimensional (2D) geometry of blades and airflow cross-section are designed using AutoCAD and CATIA while GAMBIT is employed to generate a suitable mesh for the three dimensional (3D) model. The mesh independence test is done to analyze the performance. The axial fan is simulated using FLUENT software to prove an increase in airflow rate after using the guide vane. Considering the final results, it can be observed that the airflow is increased up to 6.3%.

Keywords: Axial fan; Finite volume method; Guide vane; Numerical analysis; Turbo-dynamics.

1. INTRODUCTION

Ideally, there is no velocity component in the radial direction in axial fans, but in practice, the air leaving the axial fan has a large tangential component of velocity which produces a large amount of swirl kinetic energy. When a fluid passes through a fan the fluid is deflected generating a flow velocity with a rotational component after passage through the impeller. This rotational component forms swirl kinetic energy which is lost in the fan and reduces its efficiency. In order to solve this problem, a guide vane is designed to remove the rotational component of the air. The objective of this study is to model the axial fan and guide vane in Computational Fluid Dynamics (CFD) platform and to investigate the effect of the guide vane on the flow rate in the axial fan.

Fans are widely used in commercial and industrial applications, and consume more than 787 million kWh of energy every year in the USA, generally in space conditioning and commercial applications [1]. There are two main categories of fans classified by the path of the airflow relative to the fan: axial and centrifugal. Axial fans guide airflow into the axial direction of the fan. The pressure of air is increased by the aerodynamic lift produced in the blades, similar to the system used in an airplane wing. Axial fans are usually employed in "clean air," high volume and low-pressure applications. Axial fans are smaller and have less rotating mass compared to the centrifugal fans. Moreover, axial fans have high speed and are noisier than inline centrifugal fans of the same capacity.

Compactness, low cost and lightweight are the key benefits of axial airflow. Axial fans are commonly used in exhaust fans such as smoke, steam, and dust streams. They are suitable for ventilation applications when the reverse airflow is needed to exhaust the polluted air. Axial fans are unsuitable for systems with varying operating conditions since they have severe stall regions. Airflow is not enough in the stall region to supply the air requirement of the blades. The unstable operating condition of axial fans exhibits inefficient performance, annoying noise patterns, and accelerated drivetrain wear. This problem could be solved with an anti-stall device in many axial fans which change the airflow around the fan blades.

Tube axial fans are a type of complex propeller fan located inside a cylinder. They have better-operating efficiencies and higher pressures compared to the propeller fans since the airflow characteristics in the tube axial fans are improved. They are very useful for high airflow rate and medium-pressure applications, and because of their low rotating mass, are very suitable for HVAC systems [2].

A vane axial fan is a type of tube axial fan with outlet vanes that improve the airflow pattern. The vanes can reform the profile of airflow so that they improve the aerodynamic characteristic of the fan [3]. Vane axial fans have a low rotating mass; so, they can achieve operating speeds quite quickly as used in the boiler exhaust system and emergency ventilation. FLUENT is a cutting-edge computer program for modeling fluid flow in complex geometries. This software uses the FVM for solving the flow problems. The program provides complete mesh flexibility, solving the flow problems with unstructured meshes that

can be generated for complex geometries with relative ease. The user can create the geometry and grid by GAMBIT. Once a grid has been read into FLUENT, all remaining operations are performed within the solver. These include setting boundary conditions, defining fluid properties, executing the solution, refining the grid, and viewing and post-processing the results.

In order to achieve a successful design, parameters such as efficiency, noise, flow rate, etc. have to be considered for an axial fan as demonstrated in [4] and [5]. The designing of fans, done in the conventional design algorithms, depends intensely on the designer's experiences and skill. Therefore, this process needs trial and error to develop the best design of the fan blades shown in [6] and [7].

Several researchers work towards getting the optimum design of fan blades. Lee *et al*. [8] used an inverse method to design the axial fan. They used TURBOdesign-1 to design the axial fan for cooling condensers. Design of experiments applied to the parameters of the inverse design. By using the Response Surface Method (RSM), they carried out the axial fan with the optimum performance verified by the Air Movement and Control Association (AMCA) standards. Lee et al., in [9], presented a polynomial Response Surface Approximation (RSA) model in order to achieve the optimized axial fan. To find the best optimal design, the gradient-based search algorithm has been employed. Cho *et al*. in [10] developed a new technique by using an optimization method based on the gradient method to design the axial flow fan with efficiency and pressure selected as target objectives. They adopted 13 design variables to modify the target values, and proved their study by comparison with the experimental results which proved increased efficiency of the fans by 2.9%.

Ferro *et al*. in [11] investigated fast design methods for the Inlet Guide Vanes (IGVs) of low-cost mini-hydraulic bulb turbines. They used the classical quasi-three-dimensional analysis method for the inviscid flow through a turbomachine. This method was developed by Wu [12]. In [13], Huang and Gau studied blade designs of an axial fan using experimental and numerical methods. They employed the Levenberg-Marquardt method with a powerful algorithm in inverse design calculations. This inverse design method was used to design the shape of a gas channel for a proton exchange membrane fuel cell by Chen *et al.* [14] and Huang *et al.* [15].

Multi-objective optimizations of an axial fan blade were achieved by Kim *et al.* [16]. They selected two objectives for optimization: total efficiency and torque. They used RSA to solve the problem. This method was done by Jang and Kim in [17] and other researchers to optimize the turbo machines with specific emphasis on camber lines [18], [19], thickness location [20], Trailing Edge (TE) radius [21], and airfoil thickness [22]. For flow analysis, [10] and [16] employed CFX software. RANS equations were solved using the shear stress transport turbulence model. The simulation was validated by experimental results, [14], which was conducted with the optimized blade on the basis of the ISO 5801 standard.

In [23], Christophel *et al.* used an unstructured grid which was generated by GAMBIT and solved the Navier-Stokes (NS) equations along with the energy equation. The Re-Normalization Group (RNG) k-ε turbulence model was applied in their solution. Uniform inlet velocity was set for the inlet boundary conditions. Lee *et al.* [9] also employed the RANS equation for solving the problem. They used SST turbulence method and finite volume approximations for discretization and hexahedral grids.

In [11], Ferro *et al.* generated mesh by GAMBIT software, and used FLUENT for simulating the flow through the guide vane. They applied the standard k-ε equation for turbulent models. Also, they employed standard wall functions. Boundary conditions set by the same condition for the inlet and outlet, which were pressure inlet and pressure outlet. Radial equilibrium was used on the outlet side. In [13], the authors simulated the problem by CFD-ACE+, the commercial software introduced by ESI-CFD Inc. to solve the numerical problem. For boundary conditions, they used velocity inlet for the inlet side and pressure outlet for the outlet side. Results showed an increase in the flow rate of the designed fan blade. The original fan had better performance compared to the optimized one in higher pressures.

Aeromechanical optimization of a structural fan outlet guide vane was presented in [24]. To achieve optimization, the authors designed the guide vane to fulfill aerodynamic requirements and to satisfy a large working range and low-pressure losses. The structural analysis was performed with the software ABAQUS. CFD computation employed for calculating the aerodynamical behavior of the new guide vane design. O and H mesh topologies were used to generate the grid using Rolls-Royce grid generator PADRAM in [25]. For turbulence, the Spalart-Allmaras turbulence model was employed. The result showed that a major reduction in pressure loss will take place (approximately 20%) compared to the normal outlet guide vane.

Thakker and Hourigan [26] compared the 3D CFD analysis with the empirical performance data in a turbine with fixed guide vanes. FLUENT and GAMBIT were used to construct the model and execute the numerical simulation. Jingyin *et al.*, [27], studied variations in fan performance using the inlet box. Because of the symmetrical shape of the inlet box, only 50% of the model was meshed. The total grid number reached 2.4 million. They analyzed the flow field at peak efficiency, which was 600 kg/s. The Spalart-Allmaras method was chosen for the turbulence calculation. Comparing the result of the CFD with experimental results showed that the efficiency decreased by about 1%-4% and the overall efficiency of the fan decreased around 7% when using the inlet box.

In [28], the influence of the profile load distribution and the solidity of the outlet guide vane on outlet flow field was studied using numerical simulation. The results showed that increasing the solidity can reduce the outlet flow angle and improve the guide vane's capability of turning the flow. For the same solidity and bending angle, using the fore-load profile reduced the outlet flow angle and made the outlet flow direction closer to the axial direction. In [29], the authors described the numerical optimization of an axial fan focused on the blade and guide vane using 3D steady-state Reynolds Averaged Navier-Stokes (RANS) equations with the Shear Stress Transport (SST) turbulence model discretized by FVM. As a result of optimization, the total pressure and efficiency increased by +5.2% and +2.0%, respectively, while achieving the target total pressure.

In [30], the axial guide vane type gas liquid separator with different blade outlet angle and different number of vanes were simulated, and the pressure drop characteristics, velocity distribution as well as separation efficiency at different droplet sizes were analyzed. In [31], the authors studied the effect of inlet angle of guide vane in the Recess Vaned Casing Treatment

(RVCT). The results showed that the application of RVCT brings about noticeable improvements in the fan's stall margin and the modification of guide vane inlet angle leads to various effects.

The numerical models were developed in [32] to illustrate the effects of diffusion type guide vane cascade on Air-Cooled Steam Condenser (ACSC) performance. The simulation results showed that vane cascade can cause an increase in coolant flows across almost all fans due to its diffusion function and lower flow resistance. Meanwhile, the guide vane cascade also decreased the fan inlet temperatures because of the uniform flow field around the condenser cells. In [33], the authors provided guidance for the variable angle operation of axial-flow fans, and lays a theoretical foundation for the further studies of the evolution rules of aerodynamic noise under different blade angles. In [34], the authors studied the blade tip grooving effect on the performance of a ducted axial fan at different tip clearances in the absence and presence of IGVs. Numerical findings showed that the influence of grooving the blade on the fan parameters in the presence of guide vanes is lower than that without guide vanes.

In [35], IGVs were used as a stall control method in order to enhance the performance of a wind tunnel power fan by enlarging its surge margin. This work showed the improved surge margin of an axial flow fan used as a power fan in a wind tunnel by implementing an additional row of IGVs upstream of the rotor blades in order to redirect the entering flow to the suitable incidence angle for the rotor blades.

Widmann *et al.* [36] compared the flow through a vane-cascade swirl generator using both numerical and experimental methods. FLUENT was used for the numerical analysis. k-ε and RNG k-ε were applied to the turbulence models. The PISO algorithm was used for pressure and velocity prediction. Danczyk [37] analyzed the flow field inside an axial flow fan both experimentally and numerically. The flow field inside the axial fan was simulated by CFX-TASC flow. The simulation modeled the first stage of the fan using three stator blades and two rotor blades. Mid-span values were compared with Laser Doppler Anemometer measurements and a full three-dimensional flow field was calculated. Son *et al.* [38] studied flow characteristics and noise of axial flow fans. They designed geometry for the analysis of fan noise according to the Korean standard (KS B 6361). Two types of different axial fans were analyzed. Angular velocity is set as 204 rpm. They used the Williams and Hawking equation, presented in [39], to predict moving noise sources based on the flow similarity methods.

The direction of flow through a vane axial fan is predominantly axial. Ideally, there will be no velocity component in the radial direction. The energy transfer from the impeller to the air comes from an increase in the tangential velocity component as explained in [40]. A vane axial fan includes a set of swirl stator vanes located downstream of the impeller. These guide vanes remove the rotational component of the air, slowing it down and converting some of the excess velocity pressure into useful static pressure as shown in [41]. In [42], the authors studied the effects of inlet swirl on pressure side film cooling of neighboring vane surface. It was found out that the thermal loading on Nozzle Guide Vanes (NGVs) is highly influenced by the inlet temperature. The experimental results indicated the inlet rotating flow cannot be ignored in the real gas turbine NGVs design and the GVs are useful for periodicity quality control.

The performances of an axial pump with and without IGVs were investigated experimentally and numerically in [43]. The experimental data showed that IGVs can change the performance of axial pumps and remove the positive slope due to the backflow vortex in front of the impeller. In [44], the authors described the numerical optimization of an axial fan focused on the blade and GV using 3D steady-state RANS equations with the SST turbulence model discretized by the FVM. In addition, RSM based on the central composite design was applied to carry out the optimization. As a result of optimization, the total efficiency was improved while achieving the target total pressure.

In [45], the authors focused on the effect of IGVs on the aerodynamic performance of Multi-blade Centrifugal Fan (MCF) using RANS equations with the RNG k-ε turbulence model discretized and solved by FLUENT. The results suggested that in the MCF with IGVs, the exhaust airflow rate increases while the IGVs reduce flow loss near volute tongue areas. In [46], numerical simulation was performed for the internal 3D turbulent flow field in the two-stage axial fan using steady three-dimensional incompressible NS equations coupled with the realizable turbulent model.

In [47], the authors examined the transition process in a boundary layer on a rotor blade under the impingement of an IGV wake. The effects of wake strengths and the reduced frequency on the unsteady boundary layer development on a low-speed axial compressor were investigated using particle image velocimetry. Impingement of an IGV wake on the suction surface of a rotor blade increases the boundary layer thickness due to the negative jet effect, forcing the wake fluid away from the suction surface. In [48], based on a comparison of a fast transient of a reversible pump turbine from pump mode to generating mode with two different GV angles, it was shown how the angle affects pressure fluctuations and flow, and if the GVs are closed before the transient, fluctuations are significantly reduced. The axial flow velocity entering and leaving the fan is constant. The difference between the fluid and blade angles at the rotor entrance is known as incidence. The same difference at the trailing edge is known as a deviation. The leading edge blade angles are usually designed to match the fluid angles at the rotor inlet. A slightly positive incidence will increase the pressure rise. However, some designs incorporate a slightly negative incidence to reduce the risk of a stall condition.

The air leaving the impeller has a large tangential component which produces a large amount of swirl kinetic energy. The relative velocity vector exiting the impeller is directed at the leading edge of the stator vanes. The stator vanes, with the same geometry definitions as the impeller, transform most of velocity and kinetic swirl energy of the fluid back into static pressure. Most high-performance fans incorporate a tail cone downstream of the stator to recover some additional velocity pressure as the air expands from the annual flow area to the downstream duct area. Circular arc blading is particularly suitable for high-pressure rise units. Flat under the surface building is more appropriate for low-pressure rise units as shown in [49]. Constant thickness blades, used commonly for mixed flow fans and blowers, are not often used for high-performance vane axial fans in aircraft applications.

This study applies CFD method to analyze the improvement of the flow rate of the axial fans by using the guide vane. The two-dimensional fan blades and vane are designed in AutoCAD software and exported to CATIA in order to extend 2D sketch

to 3D. GAMBIT and FLUENT are employed to generate the grid and simulate the problem. In this study, the k-ω model was selected as the turbulence model to show the turbulent viscosity. The mesh independence test is done to analyze the performance. The axial fan is simulated using FLUENT software to prove an increase in airflow rate after using the guide vane. We fully described all of the advantages after using the guide vane compared to situations without a guide vane. Changes in velocity and pressure contours, the path line before and after using guide vanes, and the correction of velocity vectors are fully illustrated.

2. METHODOLOGY

2.1 Introduction

Figure 1 shows the work flowchart of this study. CFD are based on fundamental governing equations named continuity, momentum, and energy. The sets of these equations are chosen for the target application (incompressible, in viscid, turbulent, two or three-dimensional) i.e. the continuity equations and NS equations are required to obtain the velocity and pressure around the flow field. One of the most commonly-used discretization techniques used in CFD, the FVM, is chosen to solve these equations.

2.2 NS Equation

In physics, the motion of fluid substances is described by the NS equations. By applying Newton's second law to fluid motion, the NS equations are generated by assuming that fluid stress is a sum of pressure and viscous terms. These equations are very powerful in modeling different cases such as weather, water flow, and airflow around the wing.
Conservation of momentum (NS Equations) for incompressible flow is [50]:

$$\rho\frac{\partial u_i}{\partial t}+\frac{\partial(u_j u_i)}{\partial u_j}=-\frac{\partial p}{\partial x_i}+\frac{\partial}{\partial x_i}\left(2\mu s_{ij}\right)+\rho g_i+F_i \tag{1}$$

where F_i is the external body force and s_{ij} is the stress tensor which is given by [51]:

$$s_{ij}=\frac{1}{2}\left\{\frac{\partial u_i}{\partial x_j}+\frac{\partial u_j}{\partial x_i}\right\} \tag{2}$$

2.3 Turbulence Modeling

The purpose of the paper is to analyze the aerodynamic features of the vane axial fans. By definition, “Turbulent fluid motion is an irregular condition of flow in which the various quantities show a random variation with time and space coordinates so that statistically distinct average values can be discerned” [52]. Statistical approaches are used to express mean and fluctuating parts since the turbulence involves random fluctuations of several properties [53]. Modeling the averaged turbulence amounts is the most common engineering method to describe the turbulent flow. In this condition, the additional term known as the Reynolds stress ($\overline{u_i' u_j'}$) appears in the averaged NS equations. The Reynolds stresses should be modeled to solve the problem, and differential equations related to turbulence characteristics may have to be introduced [54].

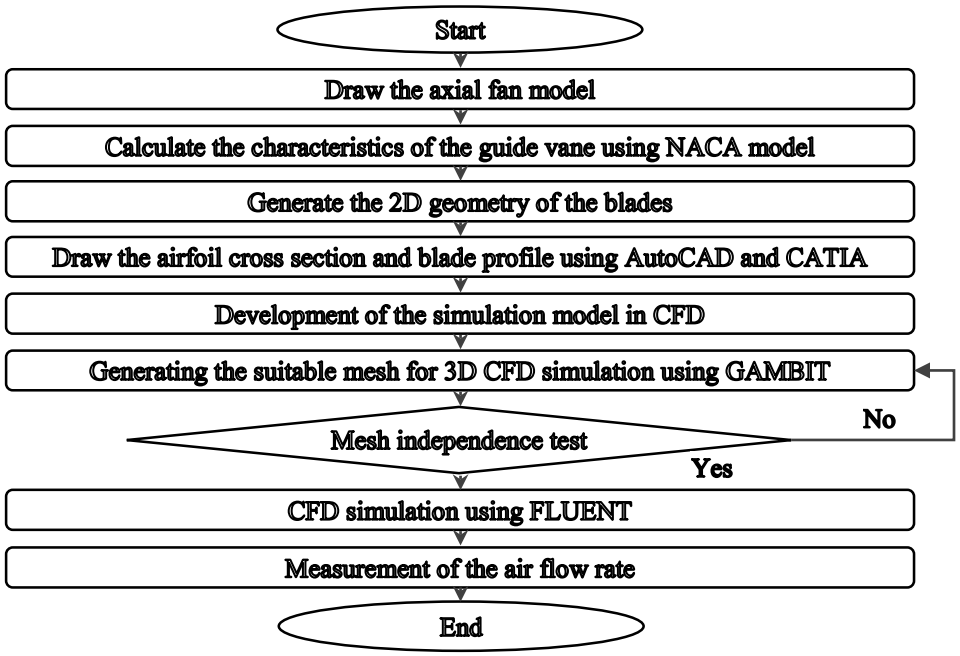

Figure 1. Procedure flowchart

$$\frac{\partial U_i}{\partial x_i} = 0 \tag{3}$$

$$u_i = U_i + u_i' \tag{4}$$

$$\rho \frac{\partial U_i}{\partial t} + \rho \frac{\partial}{\partial x_j}\left(U_i U_j + \overline{u_i' u_j'}\right) = -\frac{\partial P}{\partial x_i} + \frac{\partial}{\partial x_j}\left(2\mu S_{ij}\right) \tag{5}$$

where U is the mean velocity component, μ is the dynamic viscosity, u' is the fluctuating velocity component, which refers to instantaneous velocity u_i, and S_{ij} is the strain rate tensor. The necessity for additional stress components comes from taking moments of NS equations multiplied with fluctuating property and time average. Therefore, the Reynolds stresses equation for incompressible flow become [39]:

$$\frac{\partial \tau_{ij}}{\partial t} + U_k \frac{\partial \tau_{ij}}{\partial x_k} = -\tau_{ik}\frac{\partial U_j}{\partial x_k} - \tau_{ik}\frac{\partial U_i}{\partial x_k} + \varepsilon_{ik} + \frac{\partial}{\partial x_k}\left(\nu \frac{\partial \tau_{ij}}{\partial x_k} + C_{ijk}\right) \tag{6}$$

where:

$$\rho C_{ijk} = \rho\overline{u_i' u_j' u_k'} + \overline{P' u_i' \delta_{jk}} + \overline{P' u_j' \delta_{ik}} \tag{7}$$

and P' is the fluctuating component of pressure.

$$\varepsilon_{ij} = 2\nu \overline{\frac{\partial u_i'}{\partial x_k}} \overline{\frac{\partial u_j'}{\partial x_k}} \tag{8}$$

Because of the non-linearity of the NS equation, new unknowns are created at each level. This makes the balance between the equations and number of unknowns impossible, but some turbulence modeling is assumed for proper approximations, so a sufficient number of equations exist. The turbulence models can be categorized in four different cases according to the number of partial differential equations [53]. In this paper, two-equation models are implemented for this study:

2.3.1 Two-Equation Models

When we don't have any prior knowledge of the turbulent structure the two-equation models can be used to calculate properties of a given turbulent flow [55]. Most popular forms of these models are k-ε and k-ω models which model turbulence specific dissipation rate (ω) and dissipation rate (ε). They can be more applicable to some flows of various complexities. In this work, the Standard k-ω model will be used [56].

2.3.2 Standard k-ω Model

The standard k-ω model in ANSYS-FLUENT is based on the Wilcox k-ω model, which incorporates modifications for low Reynolds number effects, compressibility, and shear flow spreading. The Wilcox model predicts free shear flow spreading rates that are in close agreement with measurement for far wakes, mixing layers, plans and rotational cases. It is applicable to wall-bounded and free shear flows. The standard k-ω model is an empirical model based on model transport equations for the turbulence kinetic energy (k) and the specific dissipation rate (ω) which can also be thought of as the ratio of ε to k.

2.4 Design

2.4.1 Basic Airfoil Design Parameters

The simplest form of airfoil design involves starting with an assumed airfoil shape such as a National Advisory Committee for Aeronautics (NACA) airfoil. Top and Front views of airfoil parameters and geometry to explain an airfoil are demonstrated in Figures 2(a) and 2(b). Chord length is the distance between the leading and trailing edge. The chord line divides the airfoil into lower and upper surfaces. By plotting points to construct an airfoil, the points that lie between the lower and upper faces are known as the "mean camber line". "Camber" is the maximum distance between the mean camber and the central axis. "Thickness" is known as the maximum distance between the lower and upper surfaces. "Blade span" is the distance between blade tips.

2.4.2 Selection of Airfoil for Fan Blade

It is very hard to select an accurate airfoil for blade design due to the unknown relationship between maximum airflow and maximum efficiency in terms of power consumption. Each airfoil is sited on various inlet and outlet blade angles at a specific blade length, which makes the airfoil twist in shape. In this study, we selected an airfoil based on NACA standards.

Using the following equations, for a given value of x, it is possible to calculate the camber line position, y_c, the gradient of the camber line, and the thickness distribution, y_t. The position of the upper and lower surface (x_u, y_u and x_l, y_l) can then be calculated perpendicular to the camber line. In NACA four-digit airfoil profile, the first digit shows the maximum camber divided by 100. Second digit is the position of the maximum camber divided by 10. Last two digits are the thickness divided by 100. NACA 5514 which is the non-symmetrical airfoil is chosen so the maximum camber (M) thickness of the airfoil is 5% of the chord length. The distance of maximum camber (p) from the leading edge is 50% of the chord length while the maximum thickness of the airfoil is 14% of the chord length. The describing equations are given as:

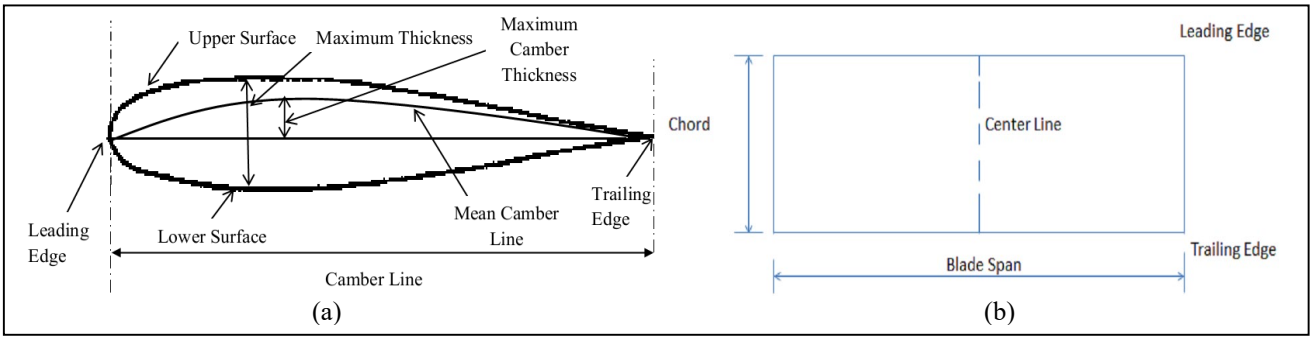

Figure 2. (a) Front view of airfoil geometry, (b) Top view of fan blade geometry

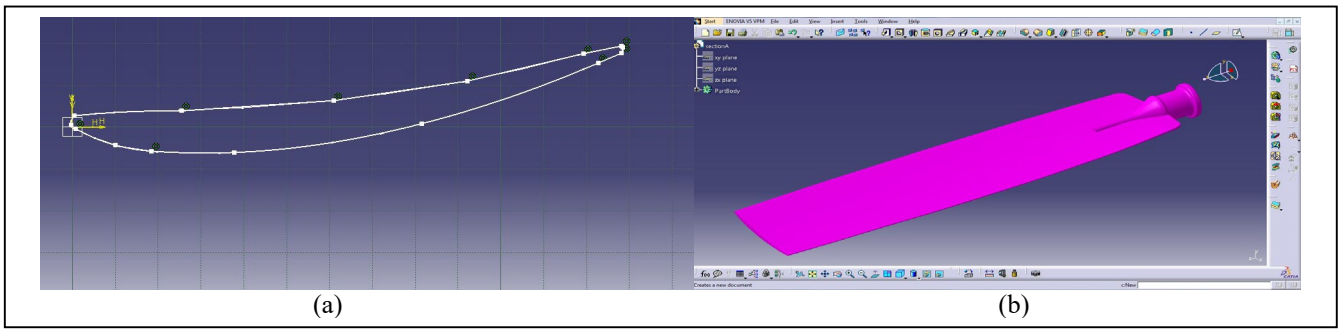

Figure 3. (a) Profile of a 2D NACA 5514 airfoil in AutoCAD, (b) 3D Blade sketch in CATIA

$$0 \le x < p \qquad p \le x < 1$$

$$y_c = \frac{M}{p^2}(2px - x^2) \qquad y_c = \frac{M}{(1-p)^2}(1 - 2p + 2px - x^2) \tag{14}$$

$$\frac{dy_c}{dx} = \frac{2M}{p^2}(p - x) \qquad \frac{dy_c}{dx} = \frac{M}{(1-p)^2}(p - x) \tag{15}$$

$$y_t = \frac{T}{0.2}(a_0 x^{0.5} + a_1 x + a_2 x^2 + a_3 x^3 + a_4 x^4) \tag{16}$$

where $a_0 = 0.2969, a_1 = -0.126, a_2 = -0.3516, a_3 = 0.2843$, and $a_4 = -0.1015$.

$$\theta = \tan\left(\frac{dy_c}{dx}\right) \tag{17}$$

$$x_u = x_c - y_t \sin(\theta) \text{ and } y_u = y_c + y_t \cos(\theta) \tag{18}$$

$$x_l = x_c + y_t \sin(\theta) \text{ and } y_l = y_c - y_t \cos(\theta) \tag{19}$$

The airfoil two-dimension profile is generated according to the above equation, which is constructed on the *x* and *y* axes with coordinates described in Table 1.

Table 1. *x* and *y* geometry of blade profile

x	1.000288	0.97654	0.907101	0.797557	0.657453	0.5	0.341204
y	0.001441	0.010095	0.0333	0.0639	0.092871	0.111764	0.114597
x	0.198246	0.08691	0.018827	0	0.030117	0.104073	0.213969
y	0.099598	0.070309	0.034451	0	-0.024902	-0.035759	-0.034147
x	0.349779	0.5	0.651564	0.790228	0.901916	0.974516	0.999712
y	-0.024146	-0.011764	-0.002421	0.001551	0.00125	-0.000546	-0.0001441

2.4.3 Construction of the 3D Models

CATIA is used as the primary software to draw a 3D model of an axial flow fan. The rotor is comprised of 12 blades and guide vane is made of 15 blades of standard NACA 5514 series blade sections. To generate a 3D fan and vane model, we first need to construct a 2D sketch of a NACA 5514 airfoil. This sketch is done in AutoCAD by importing the generated points for the NACA series. AutoCAD is one of the world's leading 2D CAD design software tools. Figure 3(a) shows the profile of a NACA 5514 airfoil in a 2D sketch in AutoCAD. Figure 3(b) shows the model of blade.

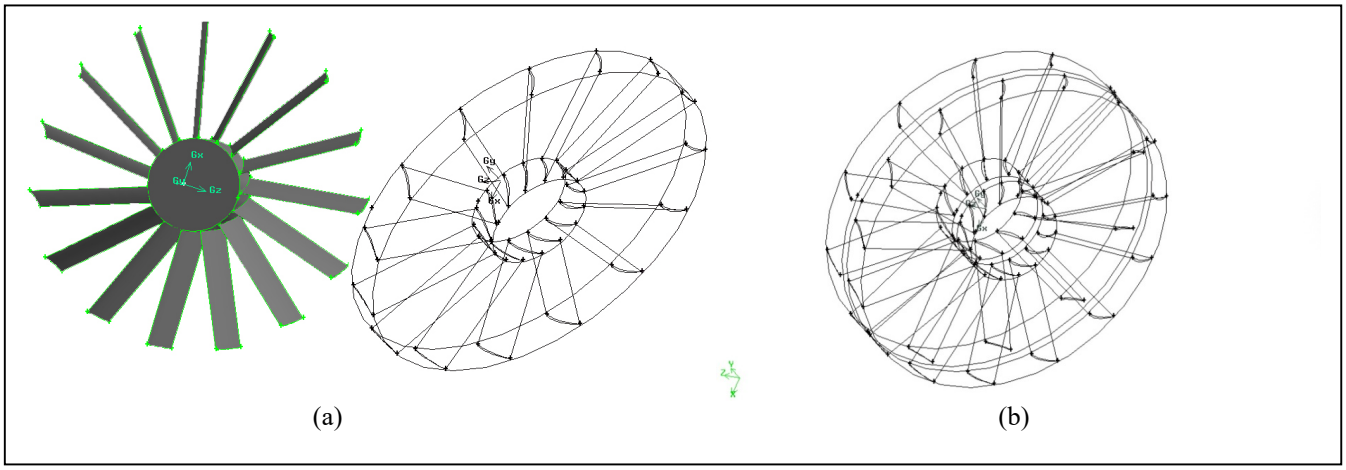

(a) (b)

Figure 4. (a) Guide vane in GAMBIT (top view), (b) Assembled fan and vane in GAMBIT

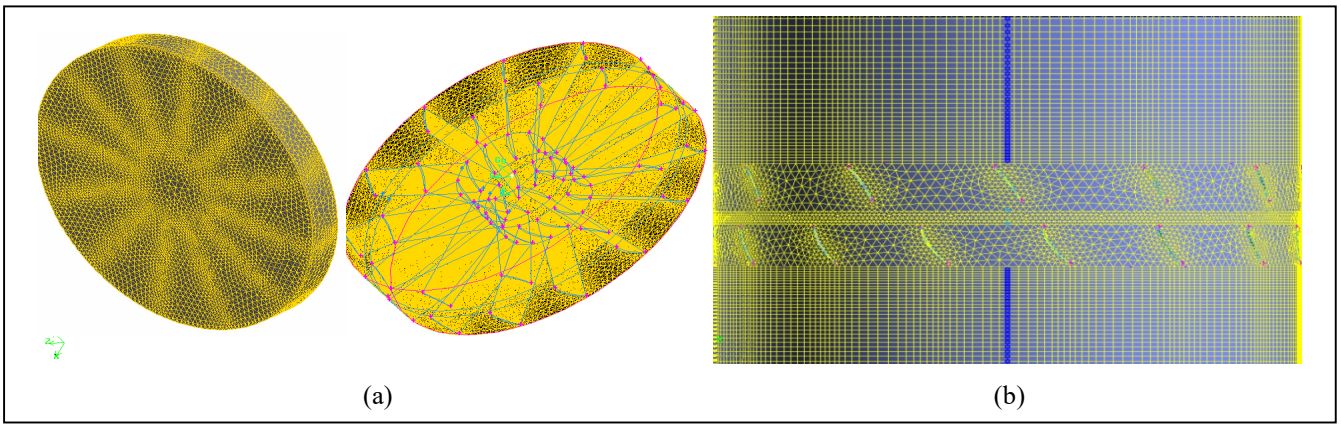

(a) (b)

Figure 5. (a) Fan mesh in blades, (b) Mesh quality around blades

The minimum length is 106 mm which is located at the tip and the maximum length of the chord is 130 mm on the hub side. The hub diameter is 350 mm and the blade length is 448 mm. The 5° twist of the blade is created by copy and rotation of the two-dimension profiles. The angle of attack on blades is 30°. Finally, a pattern command is used to generate the blades. The same steps are done for generating the guide vane but in guide vane, the cord length is 350 mm. The angle of attack is 30° without twisting. Created 3D models are exported to GAMBIT. In GAMBIT models are assembled and meshed. Figure 4(a) shows the developed 3D model of guide vane in GAMBIT.

2.5 Computational Mesh

The computational mesh of the solution domain consists of triangular prisms and tetrahedral elements. Figure 4(b) shows the axial fan assembled with guide vane in GAMBIT. After the grid independence test, the best result for the mesh is constructed by using the size function method. The starting size in size function is 10 mm and the maximum size is 25 mm. The growth rate is 1.2 to get high accuracy near the blades. Figure 5(a) and (b) show the quality of mesh using size function around the blades. To explain the variation of aerodynamic performance and getting high accuracy and reliable results, the tunnel is designed according to [38]. Vane and axial fan are located at 6250 mm from the inlet side and 12500 mm from the outlet. The number of cell elements in the whole tunnel and vane and fan domain are 3019510.

2.6 Computational Parameters

2.6.1 Fluid Model

Incompressible air is the chosen fluid in this study. For the incompressible fluid type, the density can either be constant or a predefined function of the pressure. Using air as an incompressible gas in the default FLUENT setting, the density law is defined by the Boussinesq law in which the density is kept strictly constant. With no terms in the mass and momentum equations, dependent on the temperature, the conservation equations are decoupled from the energy conservation equation.

2.6.2 Flow Model

The results are obtained with the solution of the continuity NS equations along with the equations for the selected turbulence model. In this study, the k-ω model is selected as the turbulence model which is modeled on the turbulent viscosity with two equations.

2.6.3 Boundary Conditions

As mentioned in the previous part, pressure inlet and pressure outlet are set for boundary condition. For finding the fan performance curve, five different operating conditions are assumed which are 0, 120, 224, 320, and 374 Pa for the outlet side. Inlet boundary is defined as 0 Pa for all operating conditions.

2.6.4 Numerical Scheme

For the numerical solution of momentum, turbulence kinetic energy, and turbulence dissipation rate equations and second-order upwind discretization scheme is selected. Since the flow across the fan has high rates of swirl and turbulence, and unstructured mesh is constructed in the solution domain, the flow is not aligned with the grid, thus second-order discretization is preferred for higher accuracy. The linear option is selected for the pressure interpolation scheme that simply averages the pressures in adjacent cells to obtain face pressure values. To obtain the pressure field, SIMPLE algorithm is used under the pressure-velocity coupling drop-down list. This algorithm uses a relationship between pressure and velocity corrections to enforce mass conservation and obtain a pressure field [56].

2.7 Grid Independence Test

For finding a valid solution, the grid independence test should be done to ensure that the solution not be affected by the size of the grid. Grid independence is completed to ensure that the solution is independent of the grid size. This test is done by trying to solve the same problem with a fine grid and see the variations in results.

One of the important parts of using CFD for studies concerning the technique of meshing arrangements is to ensure the results of the CFD as accurately as possible [57]. Five different mesh types are generated by GAMBIT software to ensure the high accrue independency test. Increasing the time of simulation by the number of elements is illustrated in Figure 6. Table 2 shows the variation of the mass flow rate with different sizes of mesh. As can be seen in the first three types of meshes, the results depend on the size of the mesh. Numbers 4 and 5 in Table 2 have the same result for flow with the error rate of 2%. Considering the time of simulation, Number 5 needs 900 minutes to simulate and solve the domain but this is reduced to 500 minutes in Number 4. Considering the results of Number 4 and 5, Number 4 with 1676892 elements is selected as a suitable mesh to get acceptable results for simulation with the most optimum simulation time.

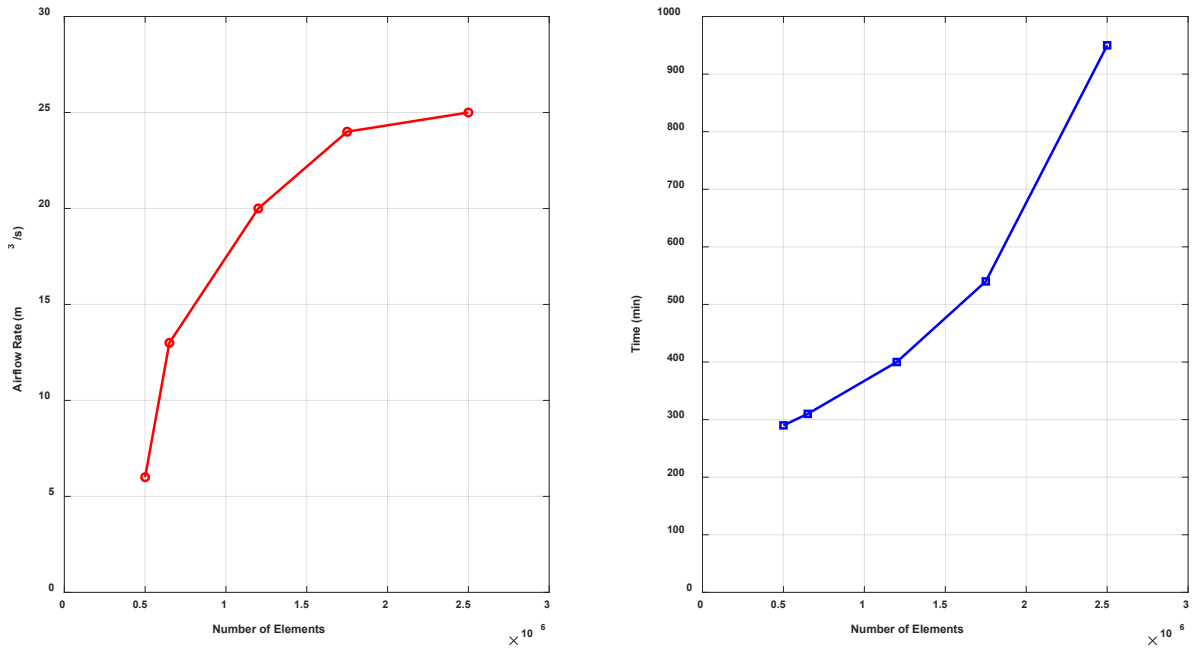

Figure 6. Variation of flow rate and computation time with numbers of elements in fan

Table 2. Grid independence test

No.	Size function			Element Numbers	Airflow Rate (m^3/s)
	Mesh Start Size	Ratio	Mesh Size (mm)		
1	40	1.2	80	385008	5.68
2	30	1.2	60	617635	13.53
3	20	1.2	50	1049428	19.64
4	10	1.2	25	1676892	23.948
5	5	1.2	10	2395542	24.506

3. RESULTS

In this section, according to the verified model, the guide vane is assembled to the axial fan. Figure 7(a) displays the final result comparisons between, after and before using guide vanes in the axial fan. After using the guide vane, the numerical simulation shows an enhancement in the air flow rate of the axial fan in all operating conditions. Figure 7(b) shows the trend of improvement in the flow rate when using the guide vane. The guide vane best performs in the highest static pressure of 6.3%. By increasing the airflow rate, the performance of the guide vane can be reduced, in the worst case, to 3.2%. Table 3 illustrates the final results of the simulation after and before using a guide vane.

Figures 8(a) and 8(b) show the different sections of the fan blade and guide vane. Plane A is the inlet of the axial fan. Plane B is the center of the blade, plane C is the middle of the vane, and finally, plane D is the outlet of the guide vane. Line x = 600 mm also is shown in Figure 8.

3.1 Velocity and Pressure

Figure 9(a) shows velocity contour on the inlet of the axial fan. This figure shows the enhancement of the velocity from center to the tip of the blades. Figure 9(b) shows the velocity contour of the blade section. The cut plane is exactly in the middle of the blades. Highest velocity is at the top of the blades in the tip section with 72 m/s. Figure 9(c) shows the velocity contour in the center cut plane in guide vane. The highest velocity in guide vanes happened on the side of 51(m/s). Figure 9(d) shows velocity contour on the outlet of the guide vane (just showing air motion). Figures 10(a) and 10(b) display that the variation domain of the axial velocity after using the guide vane becomes much less than without the guide vane. Pressure contor in the center plane of the axial fan and guide vane are shown in Figures 9(e) and 9(f).

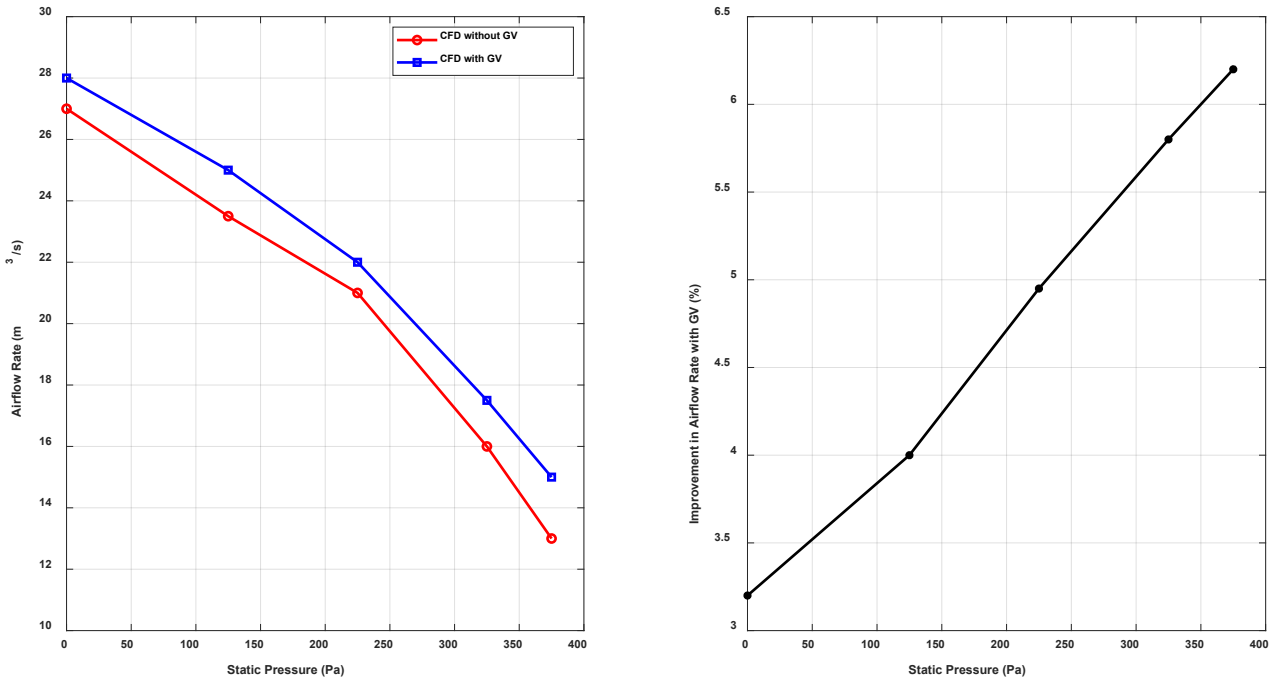

Figure 7. Static pressure vs. volume airflow rate in different simulations (Mesh 4) and percentage of improvement in airflow by using the guide vane for different static pressures in axial fan

Table 3. Final results of the air flow with guide vane

Static pressure (Pa)	Air flow without vane (m^3/s)	Airflow with vane (m^3/s)	Improvement of airflow (%)
0	27.168	28.037	3.2
120	23.948	24.9198	4
224	22.128	23.2178	4.9
320	17.808	18.8462	5.8
374	13.978	14.845	6.3

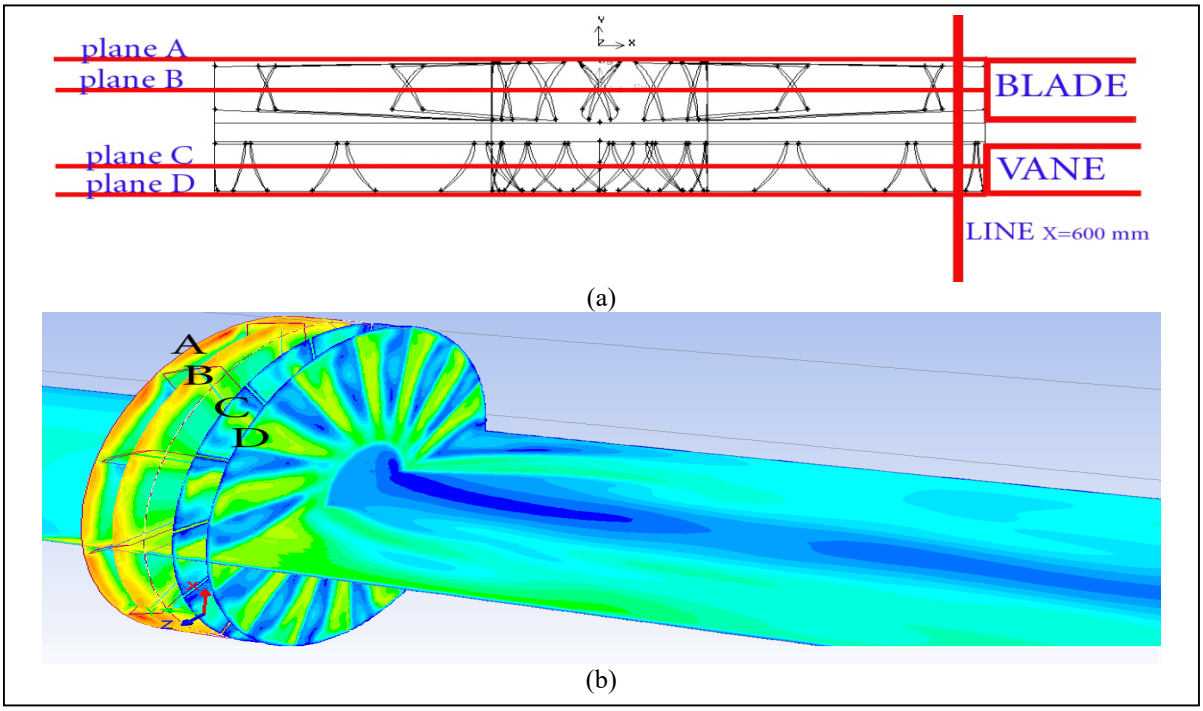

Figure 8. (a) Cutting planes, (b) Locations of the cutting planes

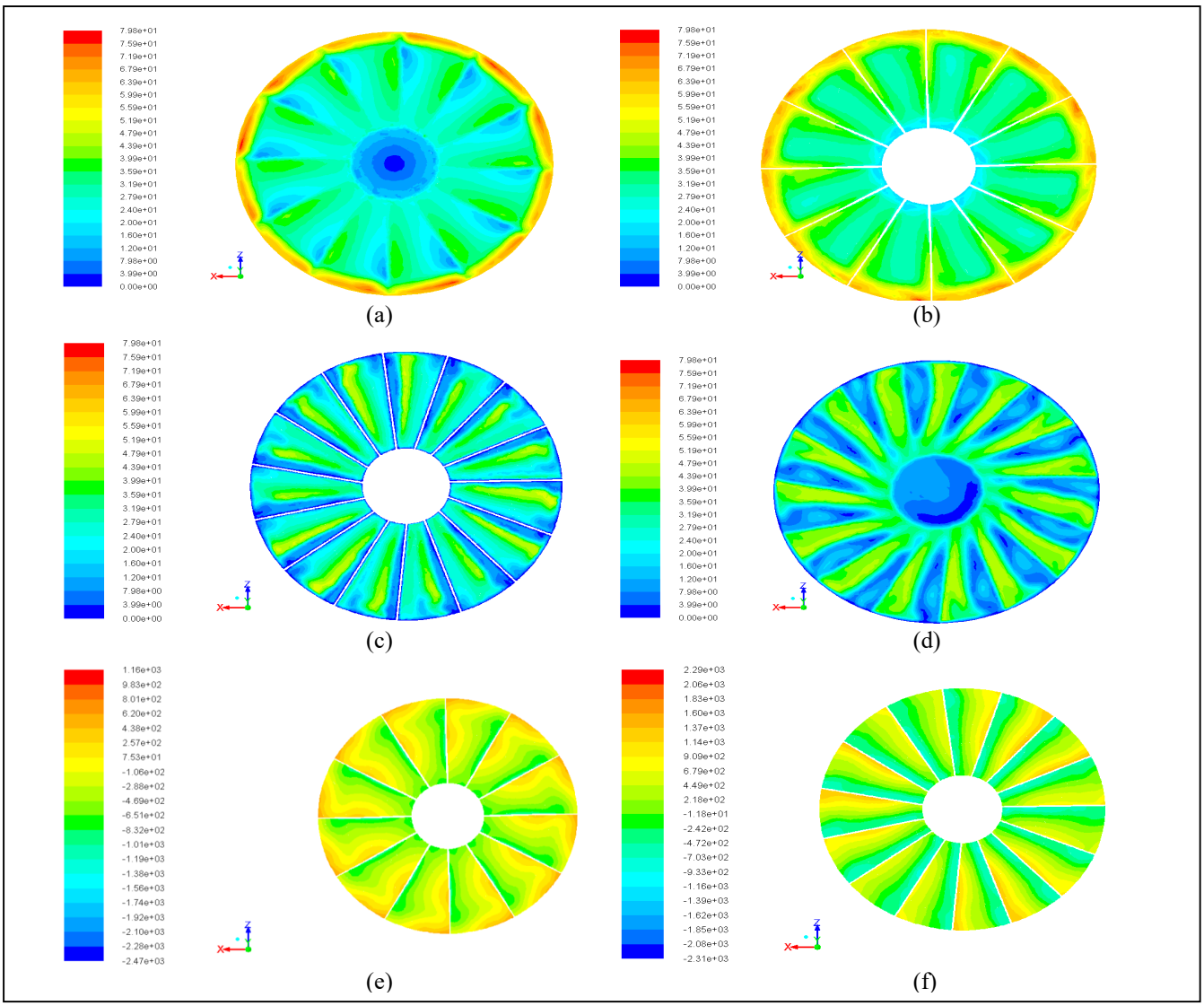

Figure 9. Velocity contour on the plane A (m/s), (b) Velocity contours on the center of the blade, plane B (m/s), (c) Velocity contour on guide vane, plane C (m/s), (d) Velocity contour on the plane D (m/s), (e) Pressure contour on guide vane, plane B (Pa), (f) Pressure contour on the plane C (Pa)

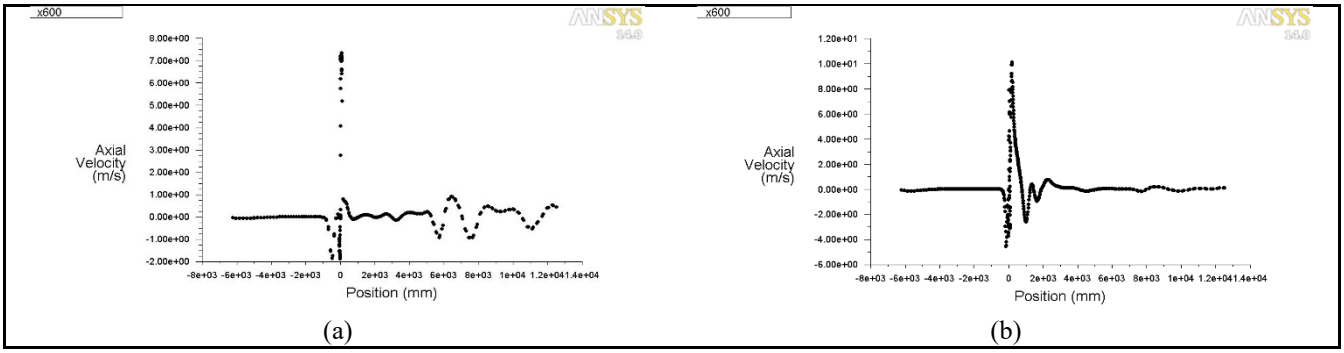

(a) (b)

Figure 10. Axial velocity at x = 600 mm (a) Without guide vane (m/s), (b) with guide vane (m/s)

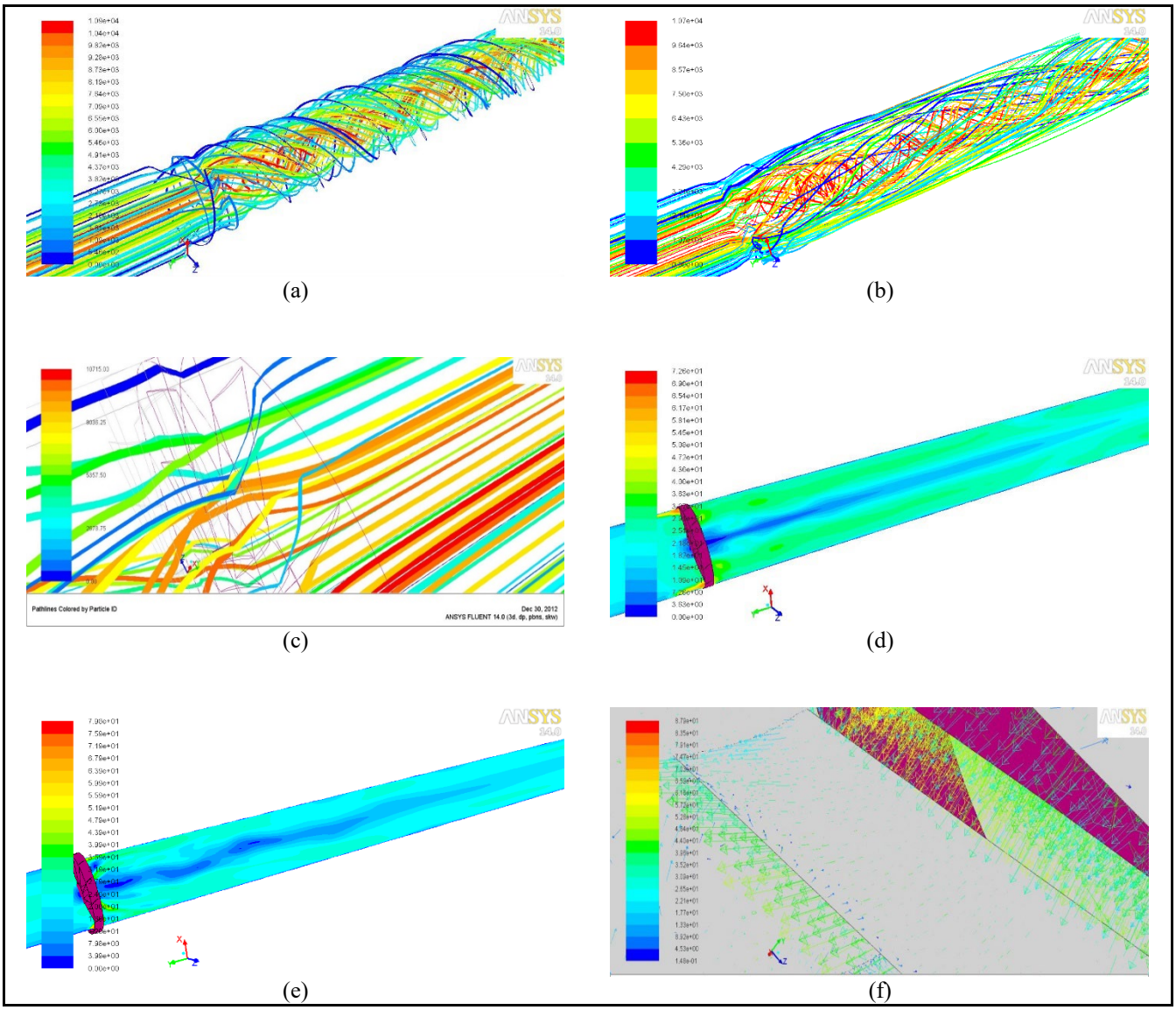

(a) (b)

(c) (d)

(e) (f)

Figure 11. (a) Path line of domain without guide vane, (b) Path line of domain with guide vane, (c) Correction of airflow direction by using guide vane, (d) Velocity contour in domain without guide vane (m/s), (e) Velocity contour of domain with guide vane (m/s), (f) Direction of vectors after designing guide vane

3.2 Path Line

Figures 11(a) and 11(b) represent the direction of airflow after fan impeller in the downstream region. There is a substantial amount of swirl kinetic energy in the axial fan without a guide vane. By using the guide vane as it can be seen in Figure 11(c) the direction of airflow becomes straight after passing through the guide vane. Figures 11(d) and 11(e) show the velocity contours before and after using the guide vane. The minimum velocity is in front of the hub. Figure 11(f) displays the correction of the direction of the velocity vectors in the outlet of the guide vane.

4. DISCUSSION

We can conclude that after designing a guide vane, the volume airflow rate increases in all of the static pressures. Also, with increasing static pressures, the improvement in airflow rate can be observed. The highest improvement of airflow can be obtained in the highest static pressure (374 Pa) with 6.3%. By increasing the amount of airflow, the performance of the guide vane is reduced. The lowest performance of the guide vane as well as the lowest improvement of airflow is 3.2% at the lowest static pressure (0 Pa) and the highest airflow rate (28.037 m^3/s). According to Figures 9 and 11, as the outlet airflow angle decreases, the outlet airflow direction approaches the axial direction. The guide vane makes use of the swirl kinetic energy and raises the pressure increase of the fan as well as its efficiency.

Considering velocity, in plane A (inlet of the axial fan) and plane B (center of the blade) the changes in the velocity is increasing radially from the core to the edges. Highest velocity is at the top of the blades in the tip section with 72 (m/s). In plane C (middle of the vane), the highest velocities can be observed on the surface of the blades, because the blades have no motion in the guide vane. A velocity contour on plane D (outlet of the guide vane) just shows the air motion.

Comparing Figures 10(a) and 10(b), we can conclude that the fluctuation domain of the axial velocity after using the guide vane reduced significantly compared to the case without using the guide vane. According to pressure contours on plane B (blades) and plane C (middle of the vane), we can see that in both cases the pressures on the blades are lower in the front than the back. The improvement in the static pressure reduces the power consumption of the fan.

According to the path line, we can see that when using a guide vane, airflow direction becomes straight compared to a situation without a guide vane in use. We can also interpret that after using a guide vane, we do not have much difference in the magnitude of velocities and, clearly, the velocity is distributed uniformly in this situation. The direction of the velocity vectors is corrected after using a guide vane so that we do not have many swirling vectors; instead, we have laminar velocity.

5. CONCLUSION

Due to the swirl kinetic energy in the downstream of axial fans, huge energy losses happen in turbo machines. To solve this problem, the guide vane is designed to reduce the effect of the swirling and transform the swirl kinetic energy into increased static pressure. In addition, by using the guide vane, the airflow in axial fans is increased. A three-dimensional model was produced using the NACA airfoil in the CATIA software and simulated with FLUENT software. Improving the airflow rate was achieved by using the guide vane for all operation conditions.

In terms of boundary conditions, we selected the pressure for the inlet as well as pressure for the outlet, since the objective of this study is to achieve volumetric airflow rate improvements. In terms of the fluid model, incompressible air is chosen as the fluid with a strictly constant density. In this study, the k-ω model was selected as the turbulence model to show the turbulent viscosity. After the grid independence test, we can find that among five different types of meshes, just numbers 4 and 5 are independent of mesh sizes. Since the time of simulation is very crucial, we selected number 4. We fully described all the advantages after using the guide vane compared to situations without a guide vane. Changes in velocity and pressure contours, the path line before and after using guide vanes, and the correction of velocity vectors are fully illustrated. The guide vane directs the fluid into the same direction of rotation as the fan impeller, which reduces the swirl kinetic energy. It can be observed that the airflow is increased up to 6.3%. The improvement in the static pressure and reduction of swirl energy increase the total fan efficiency. The results of this project's model setup can be used for future investigations of an axial flow fan using different CFD software packages such as NUMECA and Open Foam.

ACKNOWLEDGMENT

Pooya Taheri would like to thank Ms. Amy Yeung and Ms. Alison Roberts for their valuable comments. This project received no external funding.

REFERENCES

[1] R. U. Ayres, L. W. Ayres and B. Warr, Energy, power and work in the US economy, 1900-1998, *Energy*, 28(3), 2003, 219-273.

[2] US Department of Energy, *Improving Process Heating System Performance: A Sourcebook for Industry*, 2008.

[3] B. Pelley, C. Hemmelgarn, J. Althaus and J. Fries, Variable performance vane axial fan with high efficiency, *US20120128494A1 Patent*, 2011.

[4] S. Caro and S. Moreau, Aeroacoustics modeling of low pressure axial flow fans, *6th Aeroacoustics Conference and Exhibition*, Lahaina, USA 2000, 1-10.

[5] M. J. Sheu, Numerical investigation of design parameters for an axial flow cooling fan, *SAE Technical Paper*, 970933, 1997.

[6] B. Eck, R. S. Azad and D. R. Scott, *Fans; Design and Operation of Centrifugal, Axial-Flow, and Cross-Flow Fans*. Pergamon Press, 1972.

[7] S. Kalpakjian, and S. R. Schmid, *Manufacturing Processes for Engineering Materials*. Pearson, 2016.

[8] K. Y. Lee, Y. S. Choi, Y. L. Kim and J. H. Yun, Design of axial fan using inverse design method, *Journal of Mechanical Science and Technology*, 22(10), 2008, 1883-1888.

[9] K. S. Lee, K. Y. Kim and A. Samad, Design optimization of low-speed axial flow fan blade with three-dimensional RANS analysis, *Journal of Mechanical Science and Technology*, 22(10), 2008, 1864-1869.

[10] C. H. Cho, S. Y. Cho, K. Y. Ahn and Y. C. Kim, Study of an axial-type fan design technique using an optimization method, *Journal of Process Mechanical Engineering*, 223(3), 2009, 101-111.

[11] L. M. C. Ferro, L. M. C. Gato and A. F. O. Falcão, Design and experimental validation of the inlet guide vane system of a mini hydraulic bulb-turbine, *Renewable Energy*, 35(9), 2010, 1920-1928.
[12] C. H. Wu, A general though-flow theory of fluid flow with subsonic or supersonic velocity in turbomachines of arbitrary hub and casing shapes, *NACA Technical Notes*, 2302, 1951.
[13] C. H. Huang and C. W. Gau, An optimal design for axial-flow fan blade: theoretical and experimental studies, *Journal of Mechanical Science and Technology*, 26(2), 2012, 427-436.
[14] P. F. Chen, C. H. Huang, M. C. Fang and J. H. Chou, An inverse design approach in determining the optimal shape of bulbous bow with experimental verification, *Journal of Ship Research*, 50(1), 2006, 1-14.
[15] C. H. Huang, L. Y. Chen and S. Kim, An inverse geometry design problem in optimizing the shape of the gas channel for a proton exchange membrane fuel cell, *Journal of Power Sources*, 187(1), 2009, 136-147.
[16] J. H. Kim, J. H. Choi, A. Husain and K. Y. Kim, Performance enhancement of axial fan blade through multi-objective optimization techniques, *Journal of Mechanical Science and Technology*, 24(10), 2010, 2059-2066.
[17] C. M. Jang and K. Y. Kim, Optimization of a stator blade using response surface method in a single-stage transonic axial compressor, *Journal of Power and Energy*, 219(8), 2005, 595-603.
[18] S. Burguburu, C. Toussaint, C. Bonhomme and G. Leroy, Numerical optimization of turbomachinery bladings, *Journal of Turbomachinery*, 126(1), 2004, 91-100.
[19] O. Lofti, J. Teixeira, P. C. Ivey, G. Sheard and I. R. Kinghorn, Aerodynamic optimization of industrial fan blades, *ASME Turbo Expo 2005: Power for Land, Sea and Air*, Reno, NV, USA, 2005, 1-8.
[20] N. Chen, H. Zhang, H. Du, Y. Xu and W. Huang, Effect of maximum camber location on aerodynamics performance of transonic compressor blades, *ASME Turbo Expo 2005: Power for Land, Sea and Air*, Reno, NV, USA, 2005, 1-9.
[21] T. Mengistu, W. Ghaly, and T. Mansour, Aerodynamic shape optimization of turbine blades using a design-parameter-based shape representation, *ASME Turbo Expo 2007: Power for Land, Sea, and Air*, May 14-17, 2007, Montreal, Canada.
[22] C. Xu and R. Amano, A turbomachinery blade design and optimization procedure, *ASME Turbo Expo 2002: Power for Land, Sea and Air*, Amsterdam, Netherlands, 2002, 1-9.
[23] J. R. Christophel, K. A. Thole and F. J. Cunha, Cooling the tip of a turbine blade using pressure side holes-Part II: Heat transfer measurements, *Journal of Turbomachinery*, 127(2), 2005, 278-286.
[24] C. Clemen, Aero-mechanical optimization of a structural fan outlet guide vane, *Structural and Multidisciplinary Optimization*, 44(1), 2011, 125-136.
[25] S. Shahpar and L. Lapworth, PADRAM: Parametric design and rapid meshing system for turbomachinery optimization, *ASME Turbo Expo 2003: Power for Land, Sea and Air*, Atlanta, USA, 2003, 1-12.
[26] A. Thakker and F. Hourigan, Computational fluid dynamics analysis of a 0.6 m, 0.6 hub-to-tip ratio impulse turbine with fixed guide vanes, *Renewable Energy*, 30(9), 2005, 1387-1399.
[27] J. Li, H. Tian and X. Yuan, Effect of inlet box on performance of axial flow fans, *Frontiers of Energy and Power Engineering in China*, 2(4), 2008, 390-394.
[28] W. Xiao, D. Jin and X. Gui, The influence of guide vane on the performance of an axial fan for air-assisted sprayer, *Journal of Physics: Conference Series,* 1064, 2018, 012051.
[29] Y. S. Choi, Y. I. Kim, S. Kim, S. G. Lee, H. M. Yang and K. Y. Lee, Numerical simulation on the performance of axial vane type gas liquid separator with different guide vane structure, *ASME-JSME-KSME 2019 8th Joint Fluids Engineering Conference*, San Francisco, USA, 2019.
[30] Y. Fan, L. Ailan and G. Xueyan, Numerical simulation on the performance of axial vane type gas liquid separator with different guide vane structure, *International Journal of Fluid Machinery and Systems*, 10(1), 2017, 86-98.
[31] X. Chen, W. Chu, H. Zhang and X. Li, Numerical study on inlet angle of guide vane in recess vaned casing treatment, *Aerospace Science and Technology*, 93, 2019, 105323.
[32] X. Zhang, Y. Li and H. Chen, Performance assessment of air-cooled steam condenser with guide vane cascade, *Journal of Thermal Science*, 28, 2019, 993-1003.
[33] L. Wang, K. Wang, N. Wang, S. He, Y. Shi and M. Gao, 3D numerical simulation on flow field characteristic inside the large-scale adjustable blade axial-flow fan, *Proceedings of the 11th International Symposium on Heating, Ventilation and Air Conditioning (ISHVAC 2019)*, Singapore, 2019, 395-403.
[34] M. Kharati-Koopaee and H. Moallemi, Effect of blade tip grooving on the performance of an axial fan at different tip clearances in the absence and presence of inlet guide vanes, *Proceedings of the Institution of Mechanical Engineers, Part A: Journal of Power and Energy*, 234(1), 2019, 72-84.
[35] K. M. Almudahka, A. M. Elzahaby, M. K. Khalil, A. F. Nemnem and N. A. Elqussas, Enhancement of the surge margin of an axial-flow fan using inlet guide vanes (IGV), *Engineering Research Journal*, 1(39), 2019, 23-31.
[36] J. F. Widmann, S. Rao Charagundla and C. Presser, Aerodynamic study of a vane-cascade swirl generator, *Chemical Engineering Science*, 55(22), 2000, 5311-5320.
[37] S. A. Danczyk, *Experimental and computational investigation of the flow field inside an axial fan,* PhD Dissertation, Texas A&M University, 2002.
[38] Y. W. Son, J. H. Choi, J. Lee, S. R. Park, M. Kim,and J. W. Kim, Analysis and test on the flow characteristics and noise of axial flow fans, *EKC 2008 Proceedings of the EU-Korea Conference on Science and Technology*, 2008, 85-93.
[39] J. E. F. Williams and D. L. Hawkings, Sound generation by turbulence and surfaces in arbitrary motion, *Philosophical Transactions of the Royal Society of London. Series A*, *Mathematical and Physical Sciences*, 264(1151), 1969, 321-342.
[40] R. Jorgensen, *Fan Engineering*. NY: Buffalo Forge Company, 1983.
[41] W. C. Osborne, *Fans: (In Si/Metric Units)*, Pergamon Press, Oxford, 1966.

[42] Y. Li, Y. Zhang and X. Yuan, Effects of inlet swirl on pressure side film cooling of neighboring vane surface, *Proceedings of ASME Turbo Expo 2016: Turbomachinery Technical Conference and Expo*, Seoul, South Korea, 2016.
[43] Z.-W. Guo and J.-Y. Pan, The effects of the inlet guide vanes on an axial pump under off design points, *Proceedings of the ASME 2018 5th Joint US-Euro Fluids Engineering Division Summer Meeting*, Montreal, Canada, 2018.
[44] Y.-S. Choi, Y.-I. Kim, S. Kim, S.-G. Lee, H.-M. Yang and K.-Y. Lee, A study on improvement of aerodynamic performance for 100HP axial fan blade and guide vane using response surface method, *Proceedings of the ASME-JSME-KSME 2019 8th Joint Fluids Engineering Conference*, San Francisco, USA, 2019.
[45] D. Zhao, R. Chen and X.-Y. You, Numerical study of the effect of inner guide vanes on performance of multi-blade centrifugal fan of range hood, *IOP Conference Series: Earth and Environmental Science*, 332(2), 2019, 022028.
[46] J. Q. Xu, H. S. Dou, H. X. Jia, X. P. Chen, Y. K. Wei and M. W. Dong, Numerical simulation and analysis of the flow in a two-staged axial fan, *IOP Conf. Series: Materials Science and Engineering*, 129, 2016, 012060.
[47] L. Jia, T. Zou, Y. Zhu and C. Lee, Rotor boundary layer development with inlet guide vane (IGV) wake impingement, *Physics of Fluids*, 30, 2018, 040911.
[48] C. Stens and S. Riedelbauch, Influence of guide vane opening on the flow phenomena in a pump turbine during a fast transition from pump mode to generating mode, *IOP Conf. Series: Journal of Physics: Conf. Series*, 813, 2017, 012024.
[49] R. A. Wallis, *Axial Flow Fans and Ducts*. New York: Wiley, 1983.
[50] J. F. Wendt, *Computational Fluid Dynamics: An Introduction*. Springer, 2009.
[51] S. H. Liu, R. F. Huang and C. A. Lin, Computational and experimental investigations of performance curve of an axial flow fan using downstream flow resistance method, *Experimental Thermal and Fluid Science*, 34(7), 2010, 827-837.
[52] J. O. Hinze, *Turbulence*. New York: McGraw-Hill, 1975.
[53] S. Jaw and C. Chen, Present status of second-order closure turbulence models. I: overview, *Journal of Engineering Mechanics*, 124(5), 1998, 485-501.
[54] D. C. Wilcox, *Turbulence Modeling for CFD*. La Canada, Canada: DCW Industries. Inc., 2006.
[55] D. B. Spalding, Mathematical models of turbulent flames; a review, *Combustion Science and Technology,* 13(1), 1975, 3-25.
[56] Fluent 12.0 User's guide, 2009.
[57] S. B. Wibowo, Study of mesh independence on the computational model of the roll-up vortex phenomenon on fighter and delta wind models, *International Journal of Fluid Mechanics Research*, 46(5), 2019, 427-439.

APPENDIX

Table 4 provides the list of abbreviations used in this paper.

Table 4. List of Abbreviations

Abbreviation	Description
2D	Two Dimensional
3D	Three Dimensional
ACSC	Air-Cooled Steam Condenser
AMCA	Air Movement and Control Association
CFD	Computational Fluid Dynamic
FVM	Finite Volume Method
GV	Guide Vane
IGV	Inlet Guide Vane
KS	Korean Standard
MCF	Multi-blade Centrifugal Fan
NACA	National Advisory Committee for Aeronautics
NGV	Nozzle Guide Vane
NS	Navier-Stokes
RANS	Reynolds Averaged Navier-Stokes
RNG	Re-Normalization Group
RSA	Response Surface Approximation
RSM	Response Surface Method
RVCT	Recess Vaned Casing Treatment
SST	Shear Stress Transport
TE	Trailing Edge